AGU PUBLICATIONS

JGR

Journal of Geophysical Research: Atmospheres

RESEARCH ARTICLE
10.1002/2013JD021416

Key Points:
- A midlatitude barrier causes late winter maximum in high-latitude total ozone
- The maximum is primarily due to ozone buildup in the stratosphere below 500 K
- Mixing barrier effects are present in ozone observations and model simulations

Correspondence to:
J. Gille,
gille@ucar.edu

Citation:
Gille, J., S. Karol, D. Kinnison, J.-F. Lamarque, and V. Yudin (2014), The role of midlatitude mixing barriers in creating the annual variation of total ozone in high northern latitudes, *J. Geophys. Res. Atmos.*, *119*, doi:10.1002/2013JD021416.

Received 21 DEC 2013
Accepted 17 JUL 2014
Accepted article online 19 JUL 2014

The role of midlatitude mixing barriers in creating the annual variation of total ozone in high northern latitudes

John Gille[1,2], Svetlana Karol[3], Douglas Kinnison[3], Jean-Francois Lamarque[3], and Valery Yudin[3]

[1]University of Colorado, Boulder, Colorado, USA, [2]National Center for Atmospheric Research, Boulder, Colorado, USA, [3]National Center for Atmospheric Research, Boulder, Colorado, USA

Abstract Data from the HIgh Resolution Dynamics Limb Sounder (HIRDLS), the Microwave Limb Sounder (MLS), and the Whole Atmosphere Community Climate Model (WACCM) are used to investigate the annual variation of total column ozone in high northern latitudes. Downward transport of ozone-rich air by the residual mean circulation during autumn and winter bends ozone isopleths down and increases the high-latitude ozone amounts, leading to an ozone maximum at the end of the winter. During the summer months eddy mixing acts to restore pre-fall distributions of ozone. In this study the large-scale mixing in the lower stratosphere is analyzed using Nakamura's (1996) equivalent length formulation with observed and simulated ozone. The analysis of ozone mixing is performed in the tracer equivalent latitude-potential temperature coordinate system. Steep latitudinal gradients of ozone isopleths below about 500 K occur during the winter, where there are minima in the equivalent length, indicating barriers to mixing at 30°N–40°N. This transport barrier allows large ozone maxima to develop poleward of it. The barrier disappears over the summer, permitting latitudinal mixing of the high ozone air. Above 500 K mixing is more effective during the winter, so a large winter maximum does not occur. In both midlatitude and high latitude the lower stratospheric layer from 330 to 500 K doubles its ozone content from autumn to spring, compared with much smaller changes in the layer from 500 to 650 K. Our results confirm that the presence of the winter transport barrier in the lower stratosphere controls the seasonal variation of total ozone.

1. Introduction

The total amount of ozone in a vertical column above a location is important because it determines how much biologically harmful ultraviolet radiation reaches the Earth's surface. This radiation is also important for its effect on tropospheric chemistry, especially because of its role in the production of hydroxyl radicals that act to cleanse the atmosphere of many reactive species and pollutants [*Douglass et al.*, 2011]. The amount of ozone near the tropopause is particularly important for its effects on the Earth's radiation budget. For these reasons it is important to understand the distribution of ozone in the atmosphere and the factors that control its variations.

The total ozone column, denoted here by Ω, varies with latitude and season. This results from the large variation of ozone's photochemical lifetime, which is much shorter than dynamical timescales in the tropical middle stratosphere but much longer than that of the major dynamical systems at high latitudes. Here attention is focused on the annual variation of Ω at high northern latitudes, where, as has been known for many years, it increases during the autumn and winter then decreases during the spring and summer. This results in a maximum in early northern spring, and a minimum at the beginning of autumn, as shown in numerous distributions, based on both ground-based [e.g., *London*, 1980] and satellite observations [*Bowman and Krueger*, 1985; *WMO*, 1990; *Eyring et al.*, 2013].

The processes responsible for this are understood in general. In the autumn and winter the Brewer-Dobson (BD) circulation brings ozone-rich air poleward from the region in the tropical middle stratosphere where it is formed and downward into the midlatitude to high-latitude stratosphere. This overturning steepens the slopes of the ozone isopleths on a potential temperature versus latitude framework. In the absence of any barriers, the steepening is balanced by isentropic mixing, which acts to flatten these isopleths [*Holton*, 1986], preventing the BD circulation from causing large latitudinal differences in ozone mixing ratios by the end of the winter. During spring and summer the overturning ceases and mixing erases the effect of the BD circulation, bringing about the return of the isopleths to their pre-autumn positions.

In this study we look at the role played by the barrier between the midlatitude stratosphere and the subtropical troposphere that inhibits rapid mixing between these regions. The presence of such internal barriers in the atmosphere has been known for many years. Initially most attention was paid to the barrier around the polar vortex [e.g., *McIntyre and Palmer*, 1983; *Schoeberl et al*., 1992] in conjunction with studies of polar ozone destruction. Subsequently, it was recognized that the air in the tropical lower stratosphere was somewhat isolated from the midlatitudes [e.g., *Jones and Pyle*, 1984; *Randel et al*., 1993; *Volk et al*., 1996; *Plumb*, 1996] and that there was a sub-tropical barrier, due to the subtropical jet, which varies in position and intensity during the year [*Haynes and Shuckburgh*, 2000b]. *Miyazaki and Iwasaki* [2008] have analyzed the genesis of such barriers in detail, discussing mechanisms of their formation and evolution.

Strahan and Mahlman [1994] showed that the presence of such barriers was accompanied by gradients in trace species, a point also made by *Nakamura and Ma* [1997] and by *Neu et al*. [2003]. Here we ask how the transport barriers control the balance between the advection and mixing of ozone in the lower stratosphere and impact seasonal changes of the total content of ozone. To answer on these questions we employ the Modified Lagrangian Mean (MLM) approach of *Nakamura* [1995, 1996] with observed and simulated ozone distributions, making use of his diagnostics for the effective diffusivity in the lower stratosphere. *Nakamura and Ma* [1997] employed a similar strategy to study mixing and transport barriers as they affected N_2O observed by the CLAES experiment and calculated by the SKYHI model. Transforming the data onto the two-dimensional, potential temperature-equivalent latitude coordinate system, they demonstrated that the steep concentration gradients of N_2O are collocated with the locations of the calculated barriers in the middle stratosphere. *Haynes and Shuckburgh* [2000a, 2000b] subsequently studied the locations, seasonal movements, and year-to-year variability of the tracer transport barriers using an idealized tracer driven by meteorological analyses.

Here we investigate how these barriers control the annual variation of midlatitude and high-latitude Ω in the lower stratosphere bounded by the 330–500 K isosurfaces of potential temperature, and in the levels above it, in order to get a better understanding of the phase and magnitude of the seasonal variation, and the contributions of these layers to the annual cycle of Ω. These diagnostics of the role of mixing for the lower stratosphere ozone amounts at midlatitude and high latitude are complimentary to studies of *Konopka et al*. [2010] and *Ploeger et al*. [2012], who investigated the mixing of ozone from midlatitude to low latitude in the Upper Troposphere/Lower Stratosphere (UTLS).

This study makes use of the temperature and ozone data from the HIgh Resolution Dynamics Limb Sounder (HIRDLS) instrument on NASA's EOS Aura satellite, taking advantage of their unique high vertical resolution, ability to sound down to the tropopause and near-global dense coverage to provide new insights into processes in the UTLS. Data from the Ozone Monitoring Instrument (OMI), also on Aura, provide direct observations of Ω that are a check on columns calculated from HIRDLS profiles. In addition, ozone profiles observed by the Microwave Limb Sounder (MLS) on Aura and the Whole Atmosphere Community Climate Model (WACCM) results are introduced to support the picture outlined above.

The paper is organized as follows: the data are described in section 2, followed in section 3 by a discussion of the calculations with the data. Section 4 presents the annual variation seen in the HIRDLS data. The 2005–2006 HIRDLS results are compared to those from MLS and WACCM in section 5, and to HIRDLS for the 2004–2005 and 2006–2007 years in section 6. Section 7 uses these results to calculate the annual variation of ozone in different atmospheric layers in midlatitude and high latitudes, and their sum, which is compared to OMI measurements of total ozone. The findings are discussed in section 8.

2. Description of Data Used

2.1. Data Used

2.1.1. HIRDLS

HIRDLS is a 21-channel limb-scanning infrared radiometer, designed to provide global observations of temperature, 10 trace gases, aerosols, and cloud height with higher vertical resolution than previously available, down into the lowermost stratosphere with global coverage [*Gille et al*., 2003; *Gille and Barnett*, 1992]. Four channels in the 15 μm bands of CO_2 are devoted to temperature retrieval, and three in the 9.6 μm bands are used for ozone retrieval.

Unfortunately, HIRDLS suffered damage during launch, such that 80–95% of the aperture was covered, depending on channel. The optical blockage restricted viewing to 47° from the orbital plane, on the side away from the sun, limiting latitudinal coverage to 63°S to 80°N. However, the loss of capability to scan at multiple azimuths allowed all scans to be spaced ~ 100 km apart along the 14.5 scan tracks each day. Useful data collection began at the end of January 2005 and ended when the chopper failed on 17 March 2008, resulting in a data record slightly over 3 years long.

Gille et al. [2008] describe the damage, and early approaches to correcting for this optical blockage, as well as validation of the resulting Version 3 temperatures, with *Nardi et al*. [2008] discussing the validation of Version 3 (V3) ozone. Since that time work has continued to improve the quality and number of data products, resulting in the recently released Version 7 (V7) data, evaluations of which are contained in the Data Description and Quality document [*Gille and Gray*, 2013, hereafter GG] and validation papers (Gille et al., in preparation; Nardi et al., in preparation). *Khosravi et al*. [2009a, 2009b] outlined the retrieval of the profile data.

The vertical resolution of the V7 temperature data is 1 km [*Wright et al*., 2011; *Barnett et al*., 2008; *Gille et al*., 2008]. Temperature accuracy is within 1 K of radiosondes and ECMWF analyses, with a precision in the UTLS of 0.4 K [GG].

Similarly, the vertical resolution of the V7 ozone profiles is 1 km, with a precision in the UTLS, outside the tropics, of 5–10%. Below 30° latitude HIRDLS is biased high relative to sondes and MLS [GG], probably due to emission from aerosols in the tropics for which a correction has not been made. (Attempts to correct for this led to negative effects in the extra-tropical UTLS.) The V7 results used here are slightly improved over the earlier Version 6 (V6) results used in *Tegtmeier et al.*'s [2013] extensive comparison of ozone retrievals from several limb-scanning and occultation instruments. Those results show V6 HIRDLS ozone in the UTLS within ≤10% of the mean of the other instruments for latitudes ≥20°N–30°N. Comparison with SAGE II yields similar or better agreement. At higher latitudes agreement is closer to ±5%. *Neu et al*. [2014] also used V6 data and came to similar conclusions. V7 should be at least this accurate and probably somewhat better. In this study we are concentrating on regions poleward of 30°, so the low-latitude ozone was not modified.

2.1.2. Microwave Limb Sounder (MLS)

MLS measures the microwave emission from the limb of the atmosphere in numerous bands, from which vertical profiles of temperature, ozone, and several other gases and radicals are retrieved [*Waters et al*., 2006]. MLS looks forward along the orbital of Aura, resulting in 14.5 data tracks per day. This study uses V3.3 data, described in *Livesey et al*. [2011].

For temperature the vertical resolution in the UTLS is about 5 km, with a horizontal resolution of 170 km along the scan track. Temperature precision (1σ) and accuracy are ±0.4 K and +1/−2 K, respectively. Similarly, the ozone vertical resolution is 2.5 km, with a horizontal resolution of ≥300 km, with a precision and accuracy of 2–15% and 0.05 ± 5% of the values, respectively.

2.1.3. Gridded HIRDLS and MLS Data

This study utilizes the new mapped (Level 3) HIRDLS product. The data were gridded following a suggestion by *Rodgers* [1977, 2000] and implementation by *Kohri* [1981] and *Remsberg et al*. [1990] among others. The approach uses a Kalman filter, so that on each pressure surface at each latitude the time series of observations is represented as the temporally varying zonal mean plus sine and cosine coefficients of the first seven zonal waves, since there are over 14.5 orbits of data per day. The estimation is done in the forward and backward time directions, and the results combined, providing values that are Kalman smoothed in time [*Rodgers*, 2000]. This is also described in GG, which shows examples of its application to HIRDLS data. This does not affect the accuracy, but it improves the precision by about a factor of 5. Similarly, the MLS data were gridded on their pressure levels using the same mapping routine as used for HIRDLS.

Since comparisons will be made with results from the WACCM described below, which provided results on a 1.9° × 2.5° latitude vs. longitude grid, the HIRDLS and MLS data have been put on the same grid. Clearly, with only seven wave numbers, there is no information on features as small as 2.5° in longitude in the data. This resolution is used in the calculations described below to facilitate inter-comparison, and to minimize graininess in some of the results and plots. For both instruments the temperatures and pressures were then used to locate a series of potential temperature surfaces every 10 K apart, from 330 to 650 K, and the ozone was interpolated onto them.

2.1.4. Ozone Monitoring Instrument (OMI)

OMI is also flying on NASA's EOS Aura satellite with HIRDLS and MLS. *Levelt et al*. [2006] have described the instrument, which is a nadir-viewing spectrometer, measuring the upwelling reflected and scattered radiation in the UV–VIS spectral region. These measurements are retrieved to give the total column of ozone Ω using two different algorithms, including the OMI TOMS data used here. These agree with the global network of surface observations to 0.6% [*McPeters et al*., 2008; *Kroon et al*., 2008].

2.1.5. Whole Atmosphere Community Climate Model (WACCM)

The NCAR Whole Atmosphere Community Climate Model, version 4 (WACCM4), is a comprehensive numerical model spanning the range of altitudes from the Earth's surface to the thermosphere [*Garcia et al*., 2007; *Kinnison et al*., 2007; *Marsh et al*., 2013]. WACCM4 is based on the framework of the NCAR Community Atmosphere Model, version 4 (CAM4), and includes all of the physical parameterizations of CAM4 [*Neale et al*., 2013] with a finite volume dynamical core [*Lin*, 2004] for the tracer advection. In this study we compare two modes of the WACCM4. In one mode the model is driven with meteorological fields taken from the NASA Global Modeling and Assimilation Office (GMAO) Modern-Era Retrospective Analysis for Research and Applications (MERRA) [*Rienecker et al*., 2011]. Here, temperature, zonal and meridional winds, and surface pressure are used to drive the physical parameterizations that control boundary layer exchanges, advective and convective transport, and the hydrological cycle. In this mode the WACCM4 meteorological fields are "nudged" with the MERRA meteorological fields using the approach described in *Kunz et al*. [2011]. For the present study the MERRA fields were interpolated to the WACCM4 $1.9° \times 2.5°$ latitude-longitude grid. The vertical resolution in the UTLS is ~1 km. Comparisons have been made that show that the model meteorological fields (after nudging) and the MERRA meteorological fields (used to drive the model) are consistent in the UTLS region. In what follows, this mode with Specified Dynamics will be designated as SD-WACCM.

The second mode is to run WACCM in a complete self-consistent way, prescribing only the sea-surface temperatures; this is referred to as (Free-Running) FR-WACCM. Because SD-WACCM, driven by real meteorological data, was expected to be closer to the observational results, especially on dynamical processes like mixing, FR-WACCM is included to show the mixing characteristics of WACCM running in its self-consistent mode. The two modes have the same resolutions. Because FR-WACCM does not have any information about the two particular seasonal cycles studied here, any fluctuations are due to the model properties and cannot be compared to specific years. For this reason the calculations described below were carried out for each day for the 2 years, then the same days of the 2 years were averaged, although there is not a large variability from year to year. These were averaged for each month in the cross sections, and by day in the column amounts. This also results in a more averaged picture of what FR-WACCM indicates.

3. Data Analysis

In the following we will use the MLM formulation of *Nakamura* [1995, 1996] to investigate the processes controlling the seasonal variation of ozone in the lower stratosphere, seen on a potential temperature (θ) surface as a function of equivalent latitude ϕ_e.

3.1. Ozone Equivalent Latitude φ_e

Here we consider the time evolution of the zonal mean ozone on the isentropic surfaces. For a horizontal coordinate we use the tracer equivalent latitude discussed by *Allen and Nakamura* [2003]. It is analogous to the more usual equivalent latitude in terms of potential vorticity. This is permissible because the ozone is nearly monotonically increasing in latitude for $\theta \leq 500$ K, and ozone lifetimes are very long at these altitudes, making it essentially conserved. The equivalent latitude φ_e of an ozone mixing ratio contour is determined from the sum of all the areas enclosed by that contour(s) and is the latitude that encloses the same area between itself and the North Pole. In other words,

$$\varphi_e = \sin^{-1}\left(1 - A(q)/2\pi r^2\right\} \quad (1)$$

where A(q) is the area (or sum of areas) enclosed by the q contour, and r is the mean radius of the earth. In this investigation θ and φ_e were separately determined for each data source.

3.2. The Role of Isentropic Mixing

Figure 1 presents a multi-year time-latitude plot of zonal mean Ω based on OMI data. This illustrates the annual increase of Ω in the northern hemisphere during fall and winter, followed by a decrease during spring and

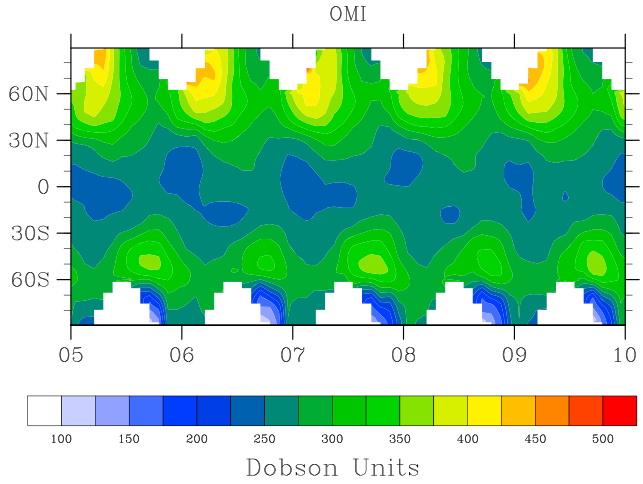

Figure 1. Latitudinal and seasonal variation of total ozone Ω measured by Ozone Monitoring Instrument (OMI) for typical years 2005–2009, illustrating the large seasonal change at high northern latitudes, and later effect at low latitudes. No smoothing has been applied. Blank regions indicate locations and times for which data are not available.

summer that restores the atmosphere to a pre-winter state. Since these are nadir-viewing UV instruments, there are no data during polar night, resulting in the white spaces on the plot. The situation in high southern latitudes is quite different because of the photochemical processes that create the "ozone hole" and is not discussed further here.

The residual mean meridional mass circulation in the stratosphere (residual mean circulation) takes air on a general path upward from the tropical tropopause, through the region of maximum ozone production in the tropics, poleward in the middle and upper stratosphere, and downward at high latitudes [*Shepherd*, 2007]. The main drive for this circulation is the breaking of extra tropical planetary waves, sometimes referred to as the extra tropical pump [*Holton et al*., 1995]. *Birner and Bönisch* [2011] show examples of the stream functions of this circulation. It brings large amounts of ozone-rich air down from the middle and upper stratosphere to the high-latitude lower stratosphere region, which could be expected to create large latitudinal gradients.

Mixing is the primary mechanism for reducing these gradients on isentropic surfaces, as described by *Holton* [1986] and others. The mixing illustrated by Holton is shown as taking place simultaneously with the overturning, thus limiting the size of the gradients that can develop.

This picture did not note the possibility of a barrier to latitudinal mixing.

3.3. Modified Lagrangian Mean (MLM) Mixing

Nakamura [1996] described a quasi-Lagrangian picture of transport on θ surfaces, using the area A enclosed by mixing ratio contours, or alternatively the equivalent latitude, as the horizontal coordinate. He considered a contour of a conserved tracer q that enclosed area A(q) between the q contour and the pole, with q increasing monotonically with increasing latitude.

Advective motions on a θ surface may distort the shape of the contour but cannot change the amount of ozone inside it; A(q) cannot change unless the contours move by diffusion, there are sources and sinks, or cross-isentropic flow.

In the absence of sources/sinks or cross-isentropic flow *Nakamura* [1996] showed that the tracer distribution in area-related coordinates is governed by the diffusion equation

$$\frac{\partial}{\partial t}\, q(A,t) = k\, \partial/\partial A \left(L_e^2\, \partial q/\partial A\right) \tag{2}$$

where

$$L_e^2\,(\mathrm{A},\mathrm{t}) = (\partial q/\partial A)^{-2}\{||\nabla q|^2\} \tag{3}$$

with L_e the equivalent length associated with the area *A*, t is the time, and *k* is the diffusion coefficient. L_e^2 was calculated by determining the gradient of the tracer at each grid point and integrating its square over the area bounded by a particular tracer contour. This quantity was then differentiated with respect to area by taking finite differences, and dividing by the square of the areal gradient of the tracer at this latitude [*Haynes and Shuckburgh*, 2000a].

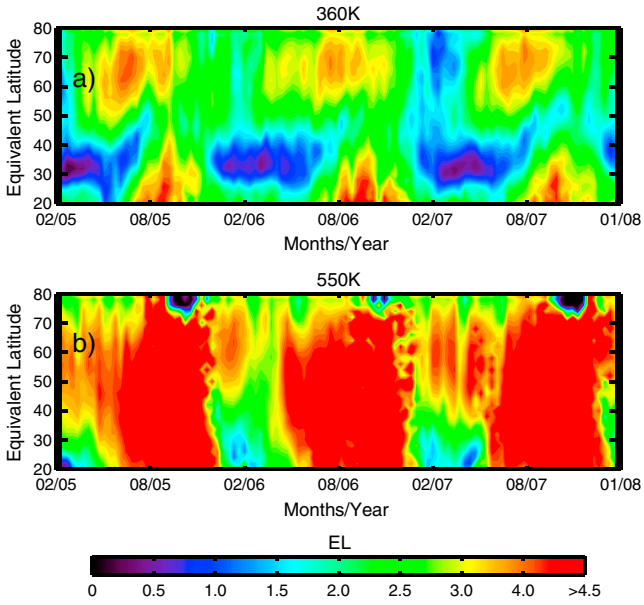

Figure 2. (a) $\Lambda = \ln (L_e / L_0)^2$ on the 360 K surface, as a function of time and equivalent latitude; (b) as Figure 2a but for the 550 K surface. (Note that these were calculated at 1° × 1° resolution, resulting in higher values of Λ than subsequent figures.)

It is convenient to normalize Le by L_0, the length of the latitude circumference where a particular Le is determined.

To determine the effective diffusivity k_{eff}, the small-scale diffusivity k should be multiplied by $(L_e / L_0)^2$ to give

$$k_{eff} = k\,(L_e/L_0)^2. \quad (4)$$

However, since k is not known, and may vary with location and time, we follow *Haynes and Shuckburgh* [2000a, 2000b] and *Shuckburgh et al.* [2001] and calculate the normalized value

$$K_{eff} = k_{eff}/k = (L_e/L_0)^2. \quad (5)$$

Because $(L_e / L_0)^2$ has a very wide range, it is usual to define $\Lambda = \ln (L_e / L_0)^2$, which is discussed in what follows.

Figure 2a shows the temporal distribution of Λ on the 360 K surface, calculated from HIRDLS ozone data, for almost the entire mission. (This calculation was done on a 1° × 1° grid, resulting in higher values of Λ than subsequent figures). Dark colors indicate regions of low Λ where mixing is slow, indicating the location of transport barriers. Yellow and red colors show regions of faster mixing.

A key feature is the region of low mixing between 30° and 40° during the winter, indicating that mixing between higher and lower latitudes is much less rapid then, and suggesting that an ozone increase poleward of the barrier will diffuse equatorward much more slowly than in the summer. This barrier has been seen in earlier analyses, by, for instance, *Nakamura and Ma* [1997], who showed the presence of low values of Λ in the sub-tropical jet position and its relationship to isopleths of N_2O for levels above 463 K. *Haynes and Shuckburgh* [2000a, 2000b] used an idealized initial tracer distribution driven by European Center for Medium-range Weather Forecasts (ECMWF) winds to demonstrate that it created barrier regions of low Λ in the winter subtropical jet location for $\theta \geq 330$ K, but with a different pattern of Λ higher altitudes. Similarly, *Allen and Nakamura* [2001] used an idealized initial tracer distribution transported by UKMO winds to create a seasonal climatology of Λ in the stratosphere that was consistent with the previous studies. In addition, they showed that the while the magnitude of Λ depends on the resolution, with higher values for finer resolution, the locations of the barriers and their relative strengths were largely independent of resolution, indicating that Λ is a robust way of displaying features important for diagnosing large-scale mixing. With the winter barrier at the jet position, we would expect to see large gradients buildup across this feature, with high values on the poleward side that would be eliminated by mixing when the barrier disappears.

By contrast, the Λ on the 550 K surface in Figure 2b does not show this 30° barrier, consistent with *Allen and Nakamura* [2001], suggesting there should be faster mixing at this level, with the absence of gradients as envisaged by *Holton* [1986] leading to the expectation of a smaller buildup during the winter at high latitudes. (While the ozone is not monotonically increasing all the way to the pole in summer, at 550 K it decreases only slightly at the highest latitudes, where the φ_e will not be completely accurate, but this does not affect φ_e at lower latitudes.) As a consequence, it should be expected that the winter buildup in the lower layers would lead to larger seasonal variations of their ozone columns than in higher layers. The next sections present evidence for these effects.

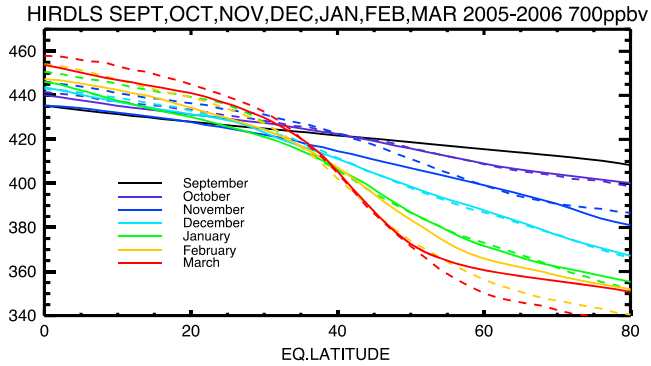

Figure 3. Observed monthly mean 700 ppb ozone isopleths for the months indicated. Solid lines—observed; dashed lines, calculated for the indicated month by vertical advection from the previous month.

4. Annual Variation of the High-latitude Ozone Column

4.1. Column Increase During Autumn and Winter of 2005–2006

The high-latitude increase of ozone is illustrated in Figure 3, where solid lines based on HIRDLS data show the monthly mean positions of the 700 ppb ozone isopleths as functions of latitude for individual months from September through March. Here the focus is on equivalent latitudes ≥ 30°. Starting from September (black line), where the isopleth has a slight downward slope toward high latitudes and is fairly straight, as the autumn and winter progress the poleward ends go down further and further, and a sharp bend or kink develops around 30°. The February and March isopleths show the limits of this process, when the isopleths have been advected down to ~ 355 K and flatten out, approaching being isentropic in high latitudes. Here, in the upper troposphere, mixing processes tend to stir ozone along isentropic surfaces. The beginning of the deviations due to mixing can be seen in January, poleward of ~ 65°.

The same picture of isopleths advected downward is found for the 1000 ppb isopleth (not shown) but with the mixing dominating closer to the 365 K level. Isopleths for lower mixing ratios become isentropic on lower surfaces and at lower latitudes.

Following *Nakamura and Ma* [1997], we do not attempt to infer or calculate the diabatic circulation but note its effect in the vertical motions of the ozone isopleths during times when it dominates the horizontal mixing. We have approximated its effects by calculating changes due to the downward motion given by the radiative cooling rates, since this gives the vertical velocity in θ-coordinates. For this calculation the WACCM code was used with HIRDLS ozone and temperature; other radiative gases were taken from WACCM. The dashed lines show the predicted position for the month of that color, based on advecting the previous month's isopleths downward. Thus, the dashed purple line indicates that the predicted October position is very close to the solid purple line, suggesting that the downward motion due to cooling has controlled the change in isopleths position. For November (darker blue) the observed and predicted positions are close, and they are in very good agreement for December and January. The agreement between the observed and predicted positions means that the largest part of the ozone changes are due to the vertical, rather than the horizontal, component of the meridional circulation. By February and March the predicted positions are well below the observed positions at the highest latitudes, as discussed above, indicating that isentropic mixing in the troposphere is counteracting the radiative sinking, and flattening the isopleths.

From April to August radiative cooling rates (north of 35°) are small, so there is little downward advection of the isopleths. In this period the radiatively predicted isopleths bear little resemblance to their observed positions. Just as the slopes of the high-latitude isopleths in February and March become small (on isentropic surfaces), all isopleths in this domain become progressively flatter with time (not shown), showing that isentropic mixing dominates during the spring and summer months.

The effect of the residual circulation on high-latitude ozone isopleths from 150 to 2600 ppb for the period from September 2005 to August 2006 is illustrated in Figure 4, where they are overplotted on the 2-D Λ field (colors) calculated from the gridded HIRDLS ozone data. The ozone isopleths in September (Figure 4a) have a very small downward tilt in the poleward direction, and all are nearly straight, as would be expected with the rapid mixing indicated by the large Λ.

By December (Figure 4b) Λ has decreased at most locations, and a barrier region has formed at the subtropical jet position, while the poleward ends of the isopleths have been advected significantly downward. More relevant to the present discussion, the lower isopleths show a significant bend or "kink" at the barrier and large gradients on the isentropes.

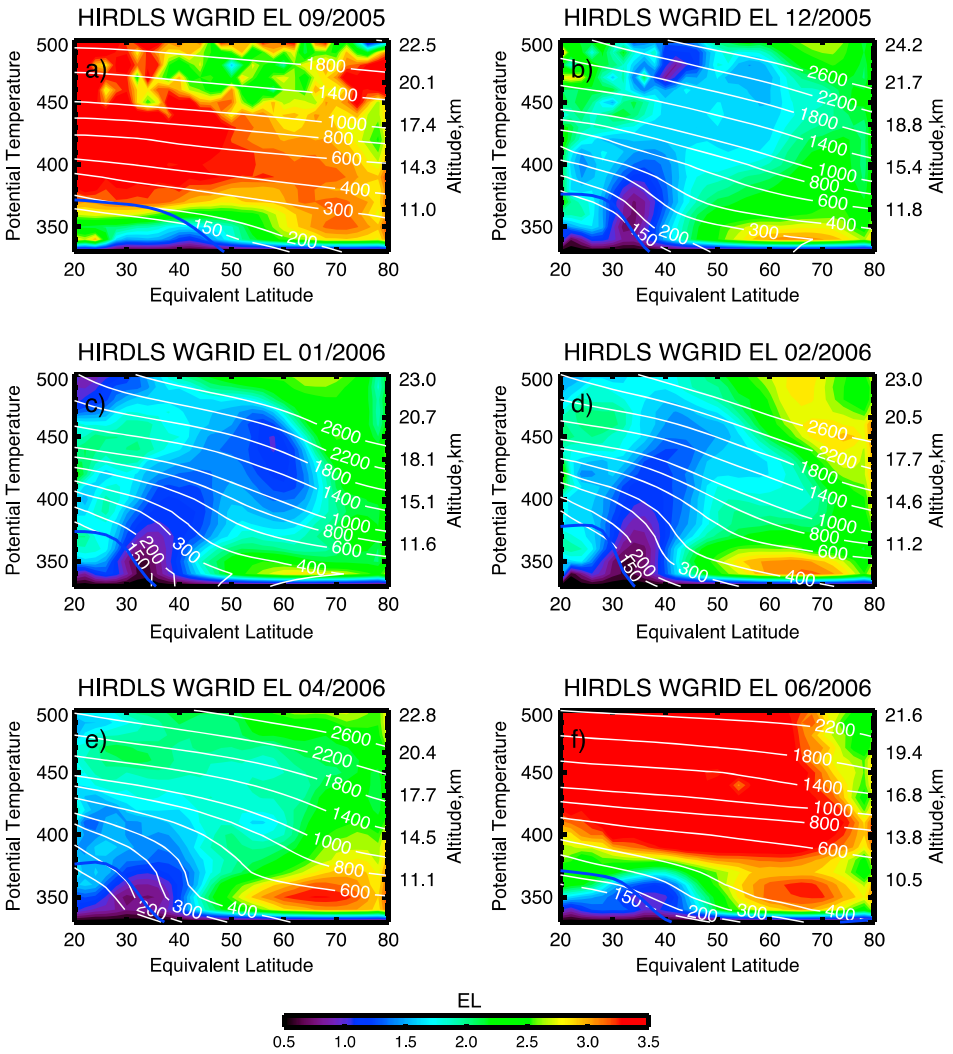

Figure 4. $\Lambda = \ln (L_e / L_0)^2$, calculated from HIgh Resolution Dynamics Limb Sounder Version 7 (HIRDLS V7) ozone data on the Whole Atmosphere Community Climate Model (WACCM) 1.9° × 2.5° latitude × longitude grid. Λ values (colors) are plotted here as functions of equivalent latitude and potential temperature, with labeled ozone isopleths superposed, for (a) September 2005, (b) December 2005, (c) January 2006, (d) February 2006, (e) April 2006, and (f) June 2006. The blue line shows the tropopause.

By January (Figure 4c) the Λ barrier extends higher, and leans poleward, while the poleward ends of the isopleths continue down, and the kinks in the lower isopleths become more pronounced. Also interesting, the upper portion of the barrier is closer to 60° equivalent latitude and extends close to 480 K, and is where some of the isopleths ≥1000 ppb have smaller kinks. This poleward tilt of Λ is also seen in *Allen and Nakamura* [2001]. Inspection of plots like those of Figure 2 for levels from 400 to 450 K indicate that the barrier near 40°N extends upward, becoming weaker and more intermittent with altitude, and another higher latitude barrier that is strongest only in the middle of the winter, possibly due to position(s) of the strongest winds at that level, in the altitude range between the sub-tropical jet and the bottom of the polar jet. This also affects the ozone gradient along isentropic surfaces, as discussed in section 5.

These trends continue into February (Figure 4d), when the lower isopleths are close to their lowest altitudes and the kinks extend up to almost 450 K. As noted above, in autumn and early winter the downward motion of the isopleths follows closely the downward velocity in isentropic coordinates given by the radiative cooling rate, reinforcing the importance of the vertical advection by the overturning circulation. However, the higher latitude (>50°) higher altitude (>450 K) barrier has weakened, and the kinks there have straightened out, suggesting an earlier return of more mixing at those levels.

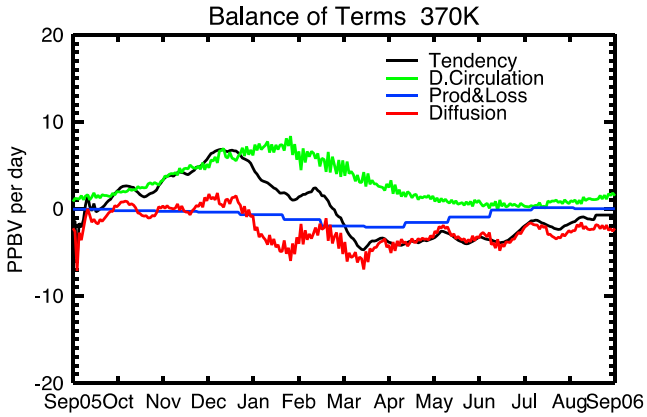

Figure 5. Terms in the continuity equation on the 370 K surface for the 40°–80°N region during 2005–2006. The ozone tendency (black) line is balanced by the vertical advection (green line, taken to be representative of the overturning circulation), chemical production minus loss (blue line), and the difference (red line), representing the diffusion.

The restoration to end-of-summer conditions, with reduced latitudinal gradients and lower ozone values, begins at the end of winter. In April (Figure 4e) overall mixing is still low, but the barrier and the kinks in the isopleths are weaker and much lower than earlier, with the poleward ends of the upper isopleths having moved higher. The rapid mixing in June (Figure 4f) has resulted in the rapid rise of the upper isopleths, and large reduction in low-altitude gradients. Changes are small into August (not shown), prior to the start of the next winter cycle. In general Figure 4 illustrates that the sharp bends or kinks occur where large gradients have built up and are mostly consistent with the location of the lowest Λs.

Because the magnitude of Λ depends on the resolution of the data, calculations were carried out for HIRDLS data on a 1° latitude by 1° longitude grid, since HIRDLS profiles are available every degree of latitude. Values of Λ (not shown) are larger, as expected, but the morphologies are very similar to those of Figures 4 and looked very similar when plotted with a color bar extending from 0.5 to 4.5, rather than to 3.5 as in Figure 4. As stated previously, the Λs are probably best understood as indicating relative differences in mixing, and regions in blue indicate regions of lower mixing but that over the monthly time scales they may still allow appreciable exchange. Similarly, they do not allow for the possibility that the diffusion coefficient k may vary with altitude or even latitude.

Since the ozone tendency is measured, and assuming the vertical transport is a reasonable approximation to the ozone change brought about by the meridional circulation, their difference gives an estimate of the effect of the diffusive mixing at levels where the chemistry is slow. Taking the entire region poleward of the barrier, 40°N to 80°N, the photochemical production minus loss from WACCM is small compared to the other terms, or has a variation through the year that is small compared to their changes, up to 480 K. The balance of the terms is clearest up to 410 K; above this level rapid temporal changes of tendency and even circulation make the balance difficult to interpret. Figure 5, for the 370 K surface, which is representative of levels from 350 to 410 K, shows that from September to December the vertical (meridional) circulation matches the tendency term, indicating that the barrier is strongly blocking mixing to lower latitudes, while from January to March the tendency decreases faster than the meridional circulation, implying that the small effective diffusivity of the barrier is not low enough to prevent the high-latitude ozone from mixing to lower latitudes. This may also reflect the effects of tropopause folds, which occur preferentially in the late winter-early spring. For the spring and summer the vertical circulation is very small, so the observed ozone decrease is due to continuing mixing to lower latitudes.

5. Comparisons With the MLS Data, and With the WACCM Model

How closely do other observations or models, and other years, show the same features seen by HIRDLS for the 2005–2006 winter?

5.1. Comparison With MLS Data

Data from MLS, which have lower vertical and along orbit resolution, have been used in the same calculations, to see how well they agree, quantitatively and qualitatively, with the HIRDLS results. The MLS data for the months of February, June, and September 2006 are shown in Figure 6 and may be compared with HIRDLS data in the corresponding frames (Figures 4d and 4f).

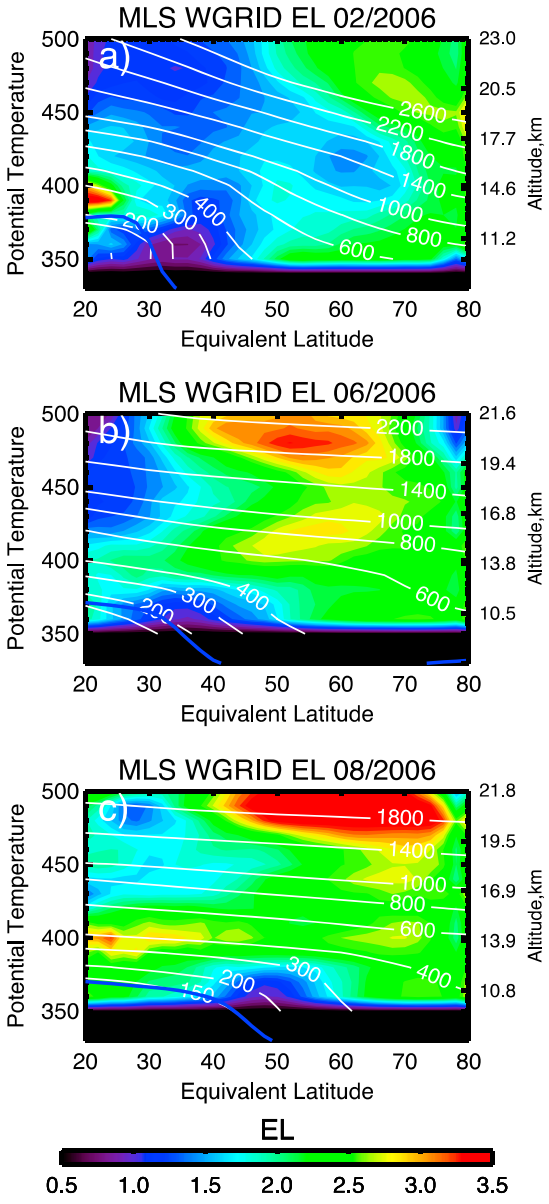

Figure 6. $\Lambda = \ln (L_e / L_0)^2$, calculated from Microwave Limb Sounder (MLS) version 3.3 ozone data on the WACCM grid. Λ values (colors) are plotted here as functions of equivalent latitude and potential temperature, with labeled ozone isopleths superposed, for (a) February 2006, (b) June 2006, and (c) August 2006. The blue line shows the tropopause. Black region below ~350 K due to unavailable data.

Looking at the February cross section (Figure 6a), the barrier that extends upward from the tropopause does not extend as high as the HIRDLS feature. However, the total region of low Λ extends much higher than that for HIRDLS, extending back toward the tropics at levels above 450 K. The low Λs in this upper region are not associated with bends in the isopleths, however. The field overall shows lower Λs than HIRDLS. The isopleths are slightly less smooth, as a result of their lower vertical resolution, but they also show the bends and steepening below about 450 K. Note also the higher altitude region of low Λ near 60°, similar to that in the HIRDLS results.

By June (Figure 6b) the isopleths above 400 K have become straighter, although the indicated Λs are still mostly lower than those based on HIRDLS. At the end of the summer, in August 2006 (Figure 6c), the MLS Λs are much larger than in February, and the isopleths above about 380 K are for the most part higher and straighter, very similar to the HIRDLS data for June 2006 (Figure 4f) or September 2005 in Figure 4a. Those below 380 K still show sharp bends that do not disappear until November.

The differences in Λs between HIRDLS and MLS can be understood in part by the difference in along track profile spacing, with HIRDLS and MLS having approximately 1° and 1.7° spacing, respectively. In addition, reducing the HIRDLS vertical resolution to that of MLS by applying the MLS vertical averaging kernels resulted in lower Λs that were more similar to MLS (not shown). Apparently, HIRDLS' higher horizontal and vertical resolutions both lead to larger Λs and greater mixing. However, MLS clearly sees the same processes at work.

5.2. Comparison With the WACCM Model

It is also of interest to see how well the two WACCM model modes capture the Λs and isopleth behavior seen in the observations. For SD-WACCM's February data (Figure 7a) the region of minimum Λ is again centered closer to 30° at the tropopause; it extends vertically, up to above 500 K, but with very low Λ below about 420 K. The isopleths in that region are bent more steeply than those shown by HIRDLS, MLS, or FR-WACCM (Figure 6b). The average of the 2 years of FR-WACCM shown in Figure 6b shows a qualitatively similar but broader vertical barrier region, again strongest to slightly above 400 K, and leaning to higher latitudes at 450 K, a feature seen by the observations but not SD-WACCM. The region of rapid mixing indicated in high latitudes of SD-WACCM is a major difference between the two WACCM modes and repeats in other years; it could result from the MERRA data driving very small ozone gradients at high latitudes that make it difficult to clearly distinguish the contours necessary for the calculation of Λ, or the way the MERRA data are used to nudge the model. This feature is also not supported

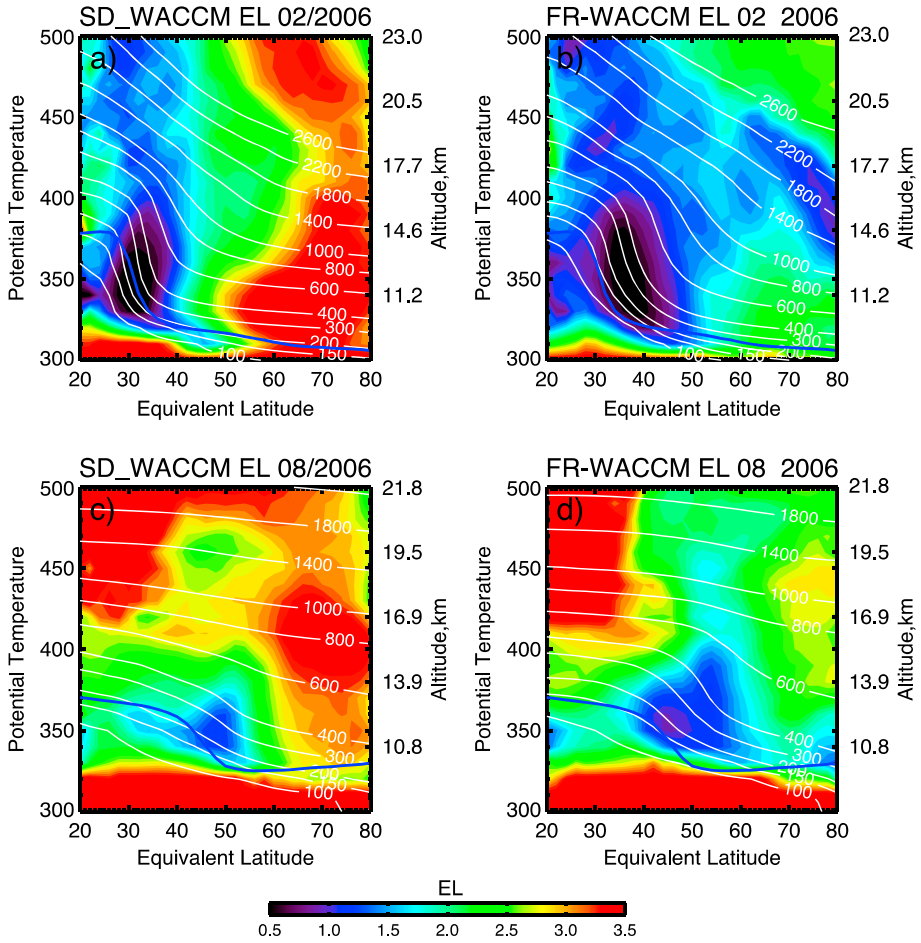

Figure 7. Λ calculated from model data on the WACCM 1.9° by 2.5° grid (WGRID). Λ values (colors) are plotted here as functions of equivalent latitude and potential temperature, with labeled ozone isopleths superposed, for February 2006, for (a) Specified Dynamics (SD)-WACCM and (b) Free-Running (FR)-WACCM; and for August for (c) SD-WACCM; and (d) FR-WACCM. The blue line shows the tropopause.

by the observations. However, this high-latitude mixing may steepen the isopleths at the barrier by eroding the sub-tropical region and squeezing the gradients into narrower latitude bands. Thus, both measurements and models show barriers extending upward from the tropopause break region. The HIRDLS Λs show a poleward tilt, as do those of MLS, but the top of the HIRDLS barrier is close to 480 K, higher than that seen by MLS or the models. Regions of lowest Λ are shown up to ~400 K for all these data.

At the end of the summer, in August, both measurements and models indicate large Λs and thus rapid mixing over the Northern Hemisphere (NH) UTLS, as shown in Figures 6c and 6d, although the models, especially FR-WACCM, still indicate a small region of low mixing extending upward from the tropopause break. The good agreement of the models and observations indicates that motions with longitudinal wavenumbers >7, which are present in the model data but not in the observations, do not materially contribute to the calculated Λ.

Latitudinal gradients provide a convenient and informative way to compare the four different views of this process. Figure 8 for February 2006 presents gradients (in ppb/degree of latitude) vs. φ_e at three levels. Figure 8a at 360 K is below the level of the tropical tropopause and is most straightforward in showing single maxima in midlatitudes. HIRDLS and MLS agree in placing this at about 35°, with a decrease north of that. FR-WACCM places its much higher maximum gradient only slightly north of this, while SD-WACCM has an even larger maximum closer to 30°. The models, especially SD-WACCM, suggest a tropical region more isolated from midlatitudes than the observations.

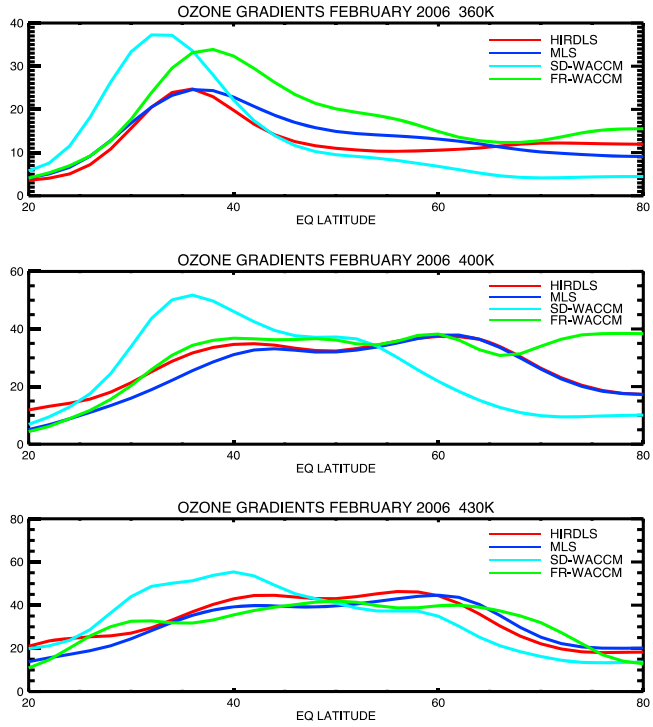

Figure 8. Latitudinal gradients of ozone mixing ratio for HIRDLS, MLS, SD-WACCM, and FR-WACCM for February 2006, for (a) 360, (b) 400, and (c) 430 K.

The gradients are larger and broader at 400 K (Figure 8b), just above the level of the tropical tropopause. Again, MLS and HIRDLS are in good agreement, with two maxima, one around 40°, another just north of 60°. FR-WACCM is in good agreement here, except for suggesting a larger gradient and lower mixing at high latitudes, while SD-WACCM again has the largest maximum (at ~ 35°), with only a hint of a second maximum, near 50°, and a very low gradient at higher latitudes, as noted above, and possibly indicating unrealistically rapid mixing there.

On the 430 K surface (Figure 8c) HIRDLS, MLS, and FR-WACCM are all in reasonable agreement, with a broad and slightly larger gradient from 40° to 60°–65°, and indications of stronger mixing at lower and higher latitudes. SD-WACCM continues to have the strongest maximum around 40°, falling to lower values at high latitudes, with a hint of a secondary maximum around 60°.

The results in this section show that HIRDLS, MLS, and the WACCM model, especially FR-WACCM see essentially the same seasonal variation, with the formation of a barrier region in midlatitudes during late autumn and winter below 450–500 K that leads to a steepening of the ozone gradient on isentropic surfaces and a winter buildup of higher values of ozone poleward of the barriers. As the barrier weakens in spring, the gradients relax to a straighter and more horizontal shape.

If WACCM had a sub-grid scale diffusivity, it would be possible to model the 2-D performance in φ_e -θ space, calculating all terms of the 2-D continuity equation [*Nakamura and Ma*, 1997], and assessing their balance. However, the finite volume dynamical core in WACCM does not have an explicit diffusion parameterization; the diffusion or smoothing is provided by the numerical schemes themselves. The resulting diffusivity is unfortunately a highly nonlinear function of the flow. Unlike the case with older, low-order centered difference schemes with explicit diffusion parameterizations, it is not possible to provide simple statements about model diffusion.

An alternate approach is to invert the 2-D continuity equation in φ_e -θ space and solve for k and k_{eff}. Since this would require not only radiative heating rates but also their vertical and latitudinal derivatives, and chemical production and loss terms, which would have to come from a model like WACCM, this is more reliably carried out using model data in a separate study.

6. Inter-annual Variation

To this point attention has been focused on the winter season from September 2005 to September 2006, but one might ask the extent to which there is inter-annual variation. HIRDLS results are used to explore this, since MLS and WACCM results are in agreement with them, as illustrated in Section 5. Figures 9a and 9b again show isopleths on Λ contours for February 2005 and 2007, respectively. The general position and shape of the midlatitude barriers are overall similar to Figure 4d although the isopleths show a stronger downward tilt toward higher latitudes, and there is an indication of a weaker barrier around 400 K. The high-altitude high-latitude isopleths show more steepening of slopes ("kinks") at the higher latitude barriers in

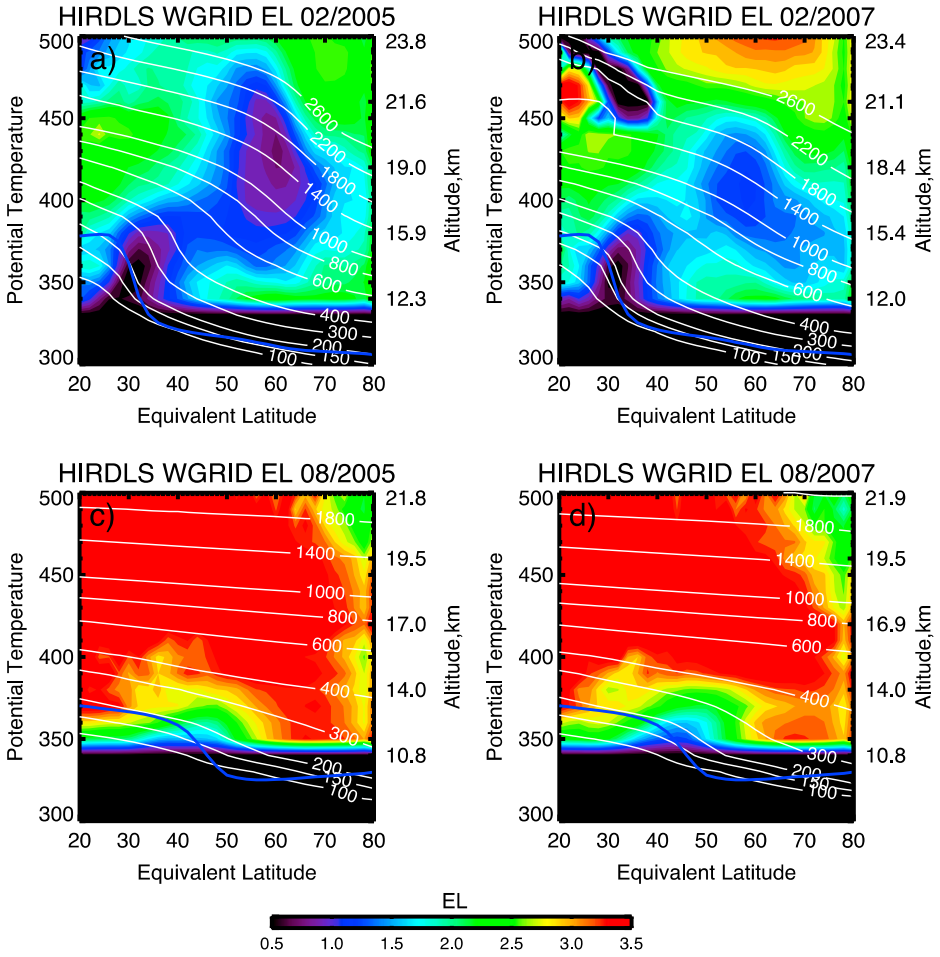

Figure 9. Λ (colors) and ozone isopleths on the WACCM grid calculated from HIRDLS V7 data for (a) February 2005, (b) February 2007, (c) August 2005, and (d) August 2007. The blue line shows the tropopause.

these years. In contrast, the August results, displayed in Figures 9c and 9d, for the same years, show little difference from the June 2006 plot.

Shuckburgh et al. [2001] investigated the effects of the quasi-biennial oscillation (QBO) on transport in the stratosphere. They found their largest effect at 624 K, well above most of the levels discussed here. The QBO at 50 hPa was in a westerly phase during the winters of 2005 and 2007, and easterly during 2006 [*Free University of Berlin*, 2014]. While suggestive, it is not clear that the differences noted above are due to the QBO, which weakens and narrows with decreasing altitude.

7. Annual Variation of Layer Amounts and Total Columns

Based on the position of the barrier, we look at the annual variation in two latitude bands, 40°N–60°N and 60°N–80°N. For vertical layers, we focus here on the layers from 330 to 650 K, where the variations are largest. The WACCM model indicates changes of only ±1–2 DU/month due to chemistry in both these levels and latitude bands, so in these locations ozone is under strong dynamical control, as seen above in Figure 5. In the following sections the variations of the ozone in a layer from 330 to 500 K, below the top of the barrier, and in a layer from 500 to 650 K, above the barrier, are calculated and compared to show the barrier effect on the size of the annual variation.

Compared to these layers, the tropospheric column below 330 K, based on SD-WACCM results, is 40 ± 3 DU during the year and has little annual variation. The layers above 650 K vary somewhat more. In the 40°–60° band that amount varies from 50 to 70 DU, with minima in January and February, and maxima in June

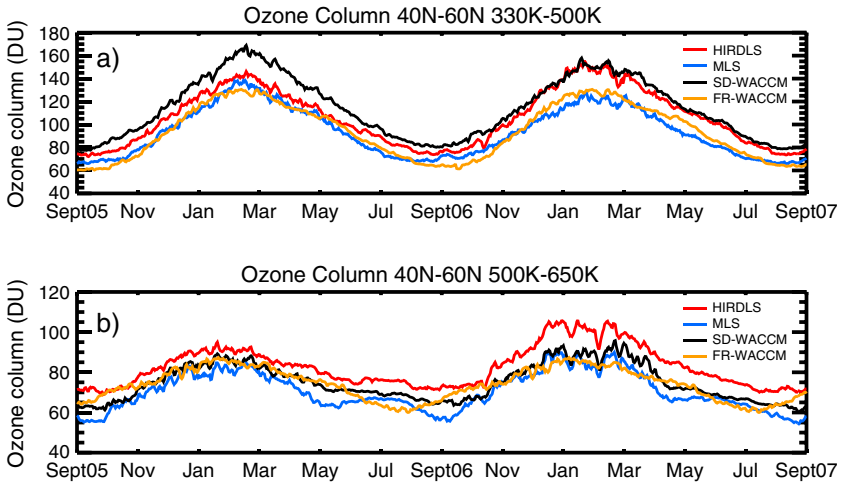

Figure 10. Annual variation of ozone amounts (in Dobson Units, DU) in different layers in the 40°N–60°N latitude region: (a) 330–500 K and (b) 500–650 K.

and July, suggesting a greater photochemical influence. From 60° to 80° the variation is from 20 to 55 DU, again with a winter/summer minimum/maximum suggesting photochemistry.

7.1. Latitude 40°N–60°N Band

Figure 10a presents the annual variations of the 330–500 K layer for two complete winter cycles covering the years 2005–2007, illustrating that in both cycles the models and measurements show the expected maxima at the end of the winter, and minima at the end of the summer, with variations of ~75 DU, or roughly a doubling of the amount in the layer. Somewhat surprisingly, SD-WACCM, driven by meteorological data, has a larger variation than the observations and FR-WACCM for 2005–2006, and larger than all but HIRDLS in 2006–2007. This may be due to SD-WACCM having a BD circulation that is too strong, or has a larger vertical ozone gradient, resulting from the MERRA data used to drive it. Its slightly higher peak during the first year may be due to that winter's Sudden Stratospheric Warming (SSW), which would be expected to bring down more ozone than a non-SSW year. It is still higher than FR-WACCM and MLS in the second year, but it is in agreement with HIRDLS, which is higher than the previous year for unknown reasons.

The phase of the maximum is slightly later in the first year than the second; this appears to be a real effect, since all three variable data sources see it. Possible causes are again the SSW, or it could be a QBO effect. The variation in the layer from 500 to 650 K illustrated in Figure 10b is much smaller, ~ 20 DU. In this level SD-WACCM is not higher than the other sources, although in the second year HIRDLS is again for unknown reasons. Because the ozone has more short-term variability, it is difficult to determine the phases of the maxima. To the extent it is possible, the phases of the two years seem more similar than in the lower level. If we take the end of summer column amounts, when the ozone has been isentropically well mixed, as a baseline, before the effects of the BD circulation and barrier have perturbed them, the amounts in this

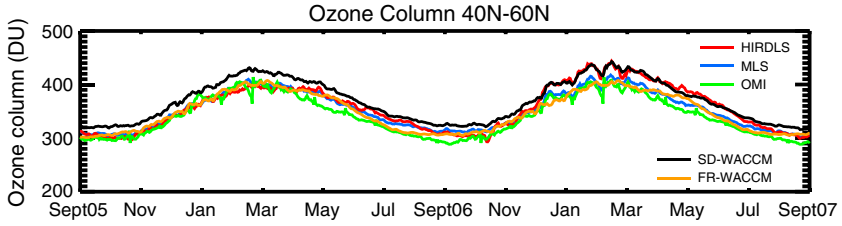

Figure 11. Annual variation of total column ozone amounts (in Dobson Units, DU) in the 40°N–60°N latitude region, determined from HIRDLS, MLS, SD-WACCM, and FR-WACCM, compared to the direct observation by OMI. Tropospheric column amounts for HIRDLS and MLS are taken from SD-WACCM.

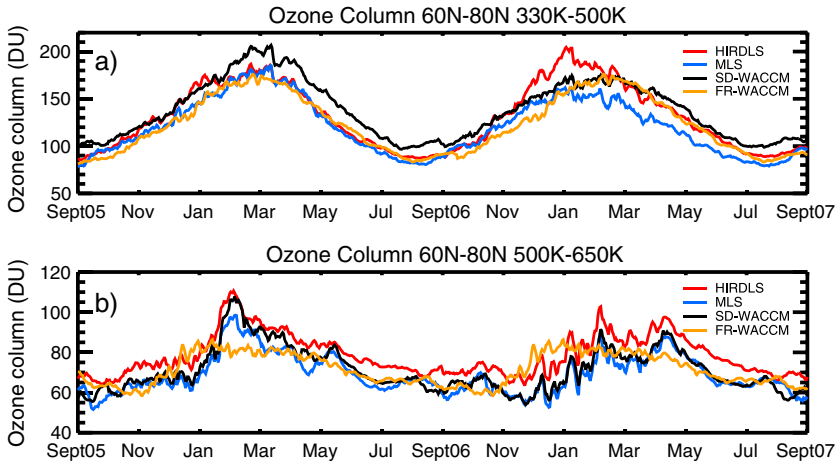

Figure 12. Annual variation of ozone amounts (in Dobson Units, DU) in different layers in the 60°N–80° N latitude region: (a) 330–500 K and (b) 500–650 K.

layer are comparable to those in the 330–500 K layer. However, the annual peak-to-peak variation is much smaller than the 330–500 K layer, supporting the hypothesis that the barrier plays an important role.

In this latitude band OMI measurements of Ω are available for the whole year and can be compared with the sum of all the layers determined by HIRDLS, MLS, and WACCM. For HIRDLS and MLS ozone columns for the layer below 330 K are taken from the SD-WACCM model and, as noted above, contribute very little to the annual variation. The comparisons are presented in Figure 11. The agreement is quite good qualitatively and even quantitatively, although in both years SD-WACCM is slightly higher, again perhaps indicating that the residual circulation is a bit too strong when driven by MERRA data compared to when it is free running. In addition, the OMI values decrease more rapidly in the late spring than the other observations and models.

7.2. Latitude 60°N–80°N Band

In this higher latitude band there is more day-to-day variability, making reliable phase determination difficult, but the same features noted in the lower latitude region can be seen. Figure 12a shows the variations in the 330–500 K layer for the 2 years. Again, the annual variation is very large, roughly a factor of 2, or close to 100 DU. Here SD-WACCM increases more than the observations or FR-WACCM in the first year, a possible SSW effect, while HIRDLS increases more than MLS or the two modes of WACCM during the second year. Overall, there appears to be good qualitative agreement.

The annual cycle is much smaller and less regular in the region above 500 K, as shown in Figure 12b. FR-WACCM, which does not include knowledge of the particular winter, does not increase as much as the observations in these winters. The observations indicate a short peak at the end of winter of the first year,

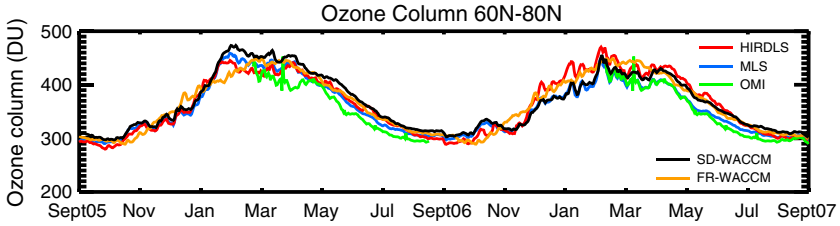

Figure 13. Annual variation of total column ozone amounts (in Dobson Units, DU) in the 60°N–80°N latitude region, determined from HIRDLS, MLS, SD-WACCM, and FR-WACCM, compared to the direct observation by OMI from March to September, when the northern polar region is illuminated. Tropospheric column amounts for HIRDLS and MLS are taken from SD-WACCM.

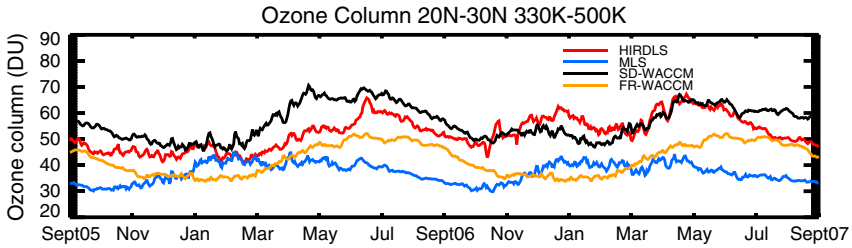

Figure 14. Annual variation of ozone amounts (in Dobson Units, DU) in different layers in the 20°N–30°N latitude region; from 330 to 500 K.

but a longer period of smaller increases during the second year. The phase is as in the 40°–60° band, although this is harder to see because of the sharp increase in February 2005.

The sum of the layers, including a tropospheric layer, as above, is shown in Figure 13.

Because this latitude band is not sunlit in winter, comparisons with OMI (in green) are only possible for the months of March through September. Once again, there is good agreement among all the sources.

7.3. Effect of the Barrier on Regions Equatorward of the Barrier

Finally, the question might be asked whether the barrier is really preventing mixing to lower latitudes. Figure 14 shows the 2 year variation of ozone in the 330–500 K layer in the 20°–30° latitude band. The observations and models agree that the variations are small, only ~ 10–20 DU. More interesting is the phase, which for all but MLS shows a maximum in May–July as the barrier weakens and mixing of ozone-rich air from higher latitudes takes place. This effect of higher values later at low latitudes can also be seen in Figure 1. The deepest minimum appears to be in January–February, when the barrier is strong. These findings are fully consistent with results obtained by *Konopka et al.* [2010] who used a model and *Ploeger et al.* [2012] who used back trajectories, to calculate ozone transport from northern hemisphere midlatitudes into the tropical tropopause layer (TTL) south of 10° or 20° φ_e, respectively. Both found mid-to late-summer maxima and February minima. They were able to ascribe the summer maximum to circulations associated with the Asian (mainly) and American monsoons. These results are in complete agreement with the picture presented in previous sections of the role of the midlatitude barrier in modulating the total ozone at midlatitude and high latitudes.

8. Summary and Conclusions

A mechanism has been presented to explain the seasonal variation of ozone at high northern latitudes. To do this, HIRDLS ozone isopleths for autumn and winter months have been plotted in an equivalent latitude-potential temperature coordinate system. During these seasons radiative cooling at high latitudes leads to air motion that advects the poleward sections of ozone isopleths downward, creating regions of steep slopes by February near 35°N, and greatly increased ozone at polar latitudes. These features and their seasonal evolution are displayed in Figures 3, 4, 6, 7, and 9 for data from HIRDLS, MLS, and two modes of the WACCM model. These slopes lead to large gradients along isentropic surfaces at levels below ~ 450 K, clearly implying the presence of a barrier to mixing, especially in contrast to higher θ levels on which the isopleths slopes are much more gradual.

Nakamura's [1996] MLM method has been used to calculate the locations and relative strengths of the barriers as minima in the normalized equivalent length diagnostic Λ. These have been calculated from the several sources of ozone data used here and plotted with the isopleths, showing that the barriers are generally stronger where the slopes of the isopleths are steepest, as would be expected.

The presence of these barriers below 450 K prevent rapid mixing to lower latitudes at these levels, leading to a larger buildup of ozone on their poleward sides during autumn and winter. Inspection of the terms indicates that the autumn buildup at 370 K is almost entirely due to the vertical transport of ozone downward, with very low mixing to lower latitudes. From February to September the diffusion is acting to reduce the ozone. The weakening and disappearance of the barrier during spring and summer then allow latitudinal mixing, the reduction of the gradients along the isentropes, and the ozone decrease at high

latitudes in this layer. At higher levels, for $\theta \geq 500$ K, the barriers are much weaker, allowing continuous mixing, and much smaller increase over the winter.

As shown in Figures 10 and 12, the annual variation is largest in the layer below 500 K where the barrier is strongest, reflecting this ozone buildup behind the barrier and its removal by mixing processes when the barrier weakens. In contrast, above the barrier there are much weaker gradients, suggesting that mixing is taking place at the same time as the overturning, resulting in a much smaller annual variation. Finally, the small, out-of-phase variation equatorward of the barrier position confirms its ability to prevent large transport from higher to lower latitudes during winter but allowing it during spring and summer.

The calculation of barrier strength based on *Nakamura*'s [1996] formulation appears to be consistent with the sharpening of the gradients at the lower altitudes, but not at the higher levels. This could indicate that the k representing small-scale mixing in equation (2) is larger at higher altitudes, as suggested by *Allen and Nakamura* [2001], and that at any rate the mixing in the region of lower Λ at these levels, although slower, is still sufficiently rapid to reduce gradients on a monthly time scale.

The differences between SD-WACCM, nudged by MERRA data, and the FR-WACCM are interesting and deserving of further study.

As shown in Figures 10–13, the models and observations show good agreement in the temporal variation of ozone in the different layers, although the Λs for the models are generally lower, suggesting slower mixing. Possible explanations may be that the differences in Λ are not large enough to make a significant difference, especially on a monthly time scale, although one would expect to see some effect in the short period variations in the layer amounts. Alternatively, it may be that diffusion, perhaps numerical, in the models makes up for the lower Λs. In any case, the models capture the seasonal variation of high-latitude ozone, as seen by HIRDLS and MLS, reasonably well.

Acknowledgments

HIRDLS and MLS data can be downloaded from the Goddard Earth Sciences Data and Information Services Center (GES DISC) (http://disc.sci.gsfc.nasa.gov/data-holdings). Model results used in the work will be made available upon request. The development of the HIRDLS data was supported in the U.S. by NASA under contract NAS5-97046, and in the U.K. by the Natural Environment Research Council. WACCM is a component of the Community Earth System Model (CESM), which is supported by the National Science Foundation (NSF) and the Office of Science of the U.S. Department of Energy. Computing resources were provided by NCAR's Climate Simulation Laboratory, sponsored by NSF and other agencies. This research was enabled by the computational and storage resources of NCAR's Computational and Information Systems Laboratory (CISL). NCAR is sponsored by the National Science Foundation (NSF). We thank the members of the HIRDLS team for their long years of effort to bring the data to this level of usefulness. We also wish to thank the reviewers, and especially one for useful and insightful comments.

References

Allen, D. R., and N. Nakamura (2001), A seasonal climatology of effective diffusivity in the stratosphere, *J. Geophys. Res.*, *106*, 7917–7935, doi:10.1029/2000JD900717.

Allen, D. R., and N. Nakamura (2003), Tracer equivalent latitude: A diagnostic tool for isentropic transport studies, *J. Atmos. Sci.*, *60*(2), 287–304, doi:10.1175/1520.

Barnett, J. J., C. L. Hepplewhite, S. Osprey, J. C. Gille, and R. Khosravi (2008), Cross-validation of HIRDLS and COSMIC radio-occultation retrievals, particularly in relation to fine vertical structure, *SPIE*, *7082*, 708216, doi:10.1117/12.800707.

Birner, T., and H. Bönisch (2011), Residual circulation trajectories and transit times into the extratropical lowermost stratosphere, *Atmos. Chem. Phys.*, *11*, 817–827, doi:10.5194/acp-11-817-2011.

Bowman, K. P., and A. J. Krueger (1985), A global climatology of total ozone from the Nimbus 7 total ozone mapping spectrometer, *J. Geophys. Res.*, *90*, 7967–7976, doi:10.1029/JD090iD05p07967.

Douglass, A., V. Fioletov, S. Godin-Beekmann, R. Muller, R. S. Stolarski, and A. Webb (2011), Stratospheric Ozone and Surface Ultraviolet Radiation. Chapter 2 in Scientific Assessment of Ozone Depletion (2010), Global Ozone Research and Monitoring Project- Report No.52, 516 pp., World Meteorol. Organ., Geneva, Switzerland.

Eyring, V., et al. (2013), Long-term ozone changes and associated climate impacts in CMIP5 simulations, *J. Geophys. Res. Atmos.*, *118*, 5029–5060, doi:10.1002/jgrd.50316.

Free University of Berlin (2014), [Available at http://www.geo.fuberlin.de/en/met/ag/strat/produkte/qbo/.]

Garcia, R. R., D. Marsh, D. E. Kinnison, B. Boville, and F. Sassi (2007), Simulations of secular trends in the middle atmosphere, 1950–2003, *J. Geophys. Res.*, *112*, D09301, doi:10.1029/2006JD007485.

Gille, J. C., and J. J. Barnett (1992), The HIgh Resolution Dynamics Limb Sounder (HIRDLS) - An instrument for the study of global change, in *The Use of EOS to Study Atmospheric Physics*, edited by J. Gille and G. Visconti, pp. 433–450, North-Holland, Amsterdam.

Gille, J., and L. Gray (2013), HIRDLS HIgh Resolution Dynamics Limb Sounder Data Description and Quality Document, Version 7 (V7). [Available at http://disc.sci.gsfc.nasa.gov/Aura/data-holdings/HIRDLS/documents/HIRDLS-V7-DQD.pdf.]

Gille, J., et al. (2003), The HIgh-Resolution Dynamics Limb Sounder (HIRDLS) experiment on AURA, in *Proceedings of SPIE*, Infrared Spaceborne Remote Sensing XI, vol. 5152, 162 pp., SPIE-The International Society for Optical Engineering, Bellingham, Washington, doi:10.1117/12.507657.

Gille, J., et al. (2008), The HIgh Resolution Dynamics Limb Sounder (HIRDLS): Experiment overview, results and validation of initial temperature data, *J. Geophys. Res.*, *113*, D16S43, doi:10.1029/2007JD008824.

Haynes, P., and E. Shuckburgh (2000a), Effective diffusivity as a diagnostic of atmospheric transport: 1. Stratosphere, *J. Geophys. Res.*, *105*(D18), 22,777–22,794, doi:10.1029/2000JD900092.

Haynes, P., and E. Shuckburgh (2000b), Effective diffusivity as a diagnostic of atmospheric transport: 2. Troposphere and lower stratosphere, *J. Geophys. Res.*, *105*(D18), 22,795–22,810, doi:10.1029/2000JD900092.

Holton, J. R. (1986), Meridional distribution of stratospheric trace constituents, *J. Atmos. Sci.*, *43*, 1238–1242, doi:10.1175/1520-0469(1986)043<1238:MDOSTC>2.0.CO;2.

Holton, J. R., P. H. Haynes, M. E. McIntyre, A. R. Douglas, R. B. Rood, and L. Pfister (1995), Stratosphere-troposphere exchange, *Rev. Geophys.*, *33*, 403–439, doi:10.1029/95RG02097.

Jones, R. L., and J. A. Pyle (1984), Observations of CH_4 and N_2O by the NIMBUS 7 SAMS: A comparison with in situ data and two-dimensional numerical model calculations, *J. Geophys. Res.*, *89*, 5263–5279, doi:10.1029/JD089iD04p05263.

Khosravi, R., et al. (2009a), Overview and characterization of retrievals of temperature, pressure, and atmospheric constituents from the HIgh Resolution Dynamics Limb Sounder (HIRDLS) measurements, *J. Geophys. Res.*, *114*, D20304, doi:10.1029/2009JD011937.
Khosravi, R., et al. (2009b), Correction to "Overview and characterization of retrievals of temperature, pressure, and atmospheric constituents from the HIgh Resolution Dynamics Limb Sounder (HIRDLS) measurements", *J. Geophys. Res.*, *114*, D23399, doi:10.1029/2009JD013507.
Kinnison, D. E., et al. (2007), Sensitivity of chemical tracers to meteorological parameters in the MOZART-3 chemical transport model, *J. Geophys. Res.*, *112*, D20302, doi:10.1029/2006JD007879.
Kohri, W. J. (1981), LRIR Observations of the Structure and Propagation of the Stationary Planetary Waves in the Northern Hemisphere during December, 1975, Cooperative Thesis No. 63, Drexel Univ. and Natl. Cent. for Atmos. Res., Boulder, Colo.
Konopka, P., J.-U. Grooß, G. Günther, F. Ploeger, R. Pommrich, R. Müller, and N. Livesey (2010), Annual cycle of ozone at and above the tropical tropopause: Observations versus simulations with the Chemical Lagrangian Model of the Stratosphere (CLaMS), *Atmos. Chem. Phys.*, *10*, 121–132.
Kroon, M., J. P. Veefkind, M. Sneep, R. D. McPeters, P. K. Bhartia, and P. F. Levelt (2008), Comparing OMI-TOMS and OMI-DOAS total ozone column data, *J. Geophys. Res.*, *113*, D16S28, doi:10.1029/2007JD008798.
Kunz, A., L. L. Pan, P. Konopka, D. E. Kinnison, and S. Tilmes (2011), Chemical and dynamical discontinuity at the extratropical tropopause based on START08 and WACCM analysis, *J. Geophys. Res.*, *116*, D24302, doi:10.1029/2011JD016686.
Levelt, P. F., et al. (2006), The ozone monitoring instrument, *IEEE Trans. Geosci. Remote Sens.*, *44*, 1093–1101, doi:10.1109/TGRS.2006.872333.
Lin, S.-J. (2004), A "vertically-Lagrangian" finite-volume dynamical core for global atmospheric models, *Mon. Weather Rev.*, *132*, 2307, doi:10.1175/15200493(2004)132<2293:AVLFDC>2.0.CO:2.
Livesey, N. J., et al. (2011), Aura Microwave Limb Sounder (MLS), 2011, Version 3.3 Level 2 data quality and description document, Version 3.3x-1.0, Jet Propul. Lab., 156 pp.
London, J. (1980), Radiative energy sources and sinks in the stratosphere and mesosphere, in *Proceedings of the NATO Advanced Study Institute on Atmospheric Ozone: Its Variations and Human Influence*, edited by Nicolet and Aiken, pp. 703–721, U. S. Department of Transportation, Washington, D. C. (Also in *WMO*, 1990).
Marsh, D. R., M. J. Mills, D. E. Kinnison, J.-F. Lamarque, N. Calvo, and L. M. Polvani (2013), Climate change from 1850 to 2005 simulated in CESM1(WACCM), *J. Clim.*, *26*(19), 7372–7391, doi:10.1175/JCLI-D-12-00558.1.
McIntyre, M. E., and T. N. Palmer (1983), Breaking planetary waves in the stratosphere, *Nature*, *305*, 593–600.
McPeters, R., M. Kroon, G. Labow, E. Brinksma, D. Balis, I. Petropavlovskikh, J. P. Veefkind, P. K. Bhartia, and P. F. Levelt (2008), Validation of the aura ozone monitoring instrument total column ozone product, *J. Geophys. Res.*, *113*, D15S14, doi:10.1029/2007JD008802.
Miyazaki, K., and T. Iwasaki (2008), Diagnosis of meridional ozone transport based on mass-weighted isentropic zonal means, *J. Atmos. Sci.*, *62*, 1192–1208, doi:10.1175/2007JAS403.1.
Nakamura, N. (1995), Modified Lagrangian-mean diagnostics of the stratospheric polar vortices Part I. Formulation and analysis of GFCL SKYHI GCM, *J. Atmos. Sci.*, *52*, 2096–2108.
Nakamura, N. (1996), Two-dimensional mixing, edge formation, and permeability diagnosed in an area coordinate, *J. Atmos. Sci.*, *53*, 1524–1537, doi:10.1175/1520-0469(1996)053<1524:TDMEFA>2.0.CO;2.
Nakamura, N., and J. Ma (1997), Modified Lagrangian-mean diagnostics of the stratospheric polar vortices: 2. Nitrous oxide and seasonal barrier migration in the cryogenic limb array etalon spectrometer and SKYHI general circulation model, *J. Geophys. Res.*, *102*, 25,721–25,735, doi:10.1029/97JD02153.
Nardi, B., et al. (2008), Validation of HIRDLS ozone measurements, *J. Geophys. Res.*, *113*, D15S03, doi:10.1029/2007JD008837.
Neale, R. B., J. Richter, S. Park, P. H. Lauritzen, S. J. Vavrus, P. J. Rasch, and M. Zhang (2013), The mean climate of the Community Atmosphere Model (CAM4) in forced SST and fully coupled experiments, *J. Clim.*, *26*(14), 5150–5168, doi:10.1175/JCLI-D-12-00236.1.
Neu, J. L., L. C. Sparling, and R. A. Plumb (2003), Variability of the subtropical "edges" in the stratosphere, *J. Geophys. Res.*, *108*(D15), 4482, doi:10.1029/2002JD002706.
Neu, J. L., et al. (2014), The SPARC Data Initiative: Comparison of upper troposphere/lower stratosphere ozone climatologies from limb-viewing instruments and the nadir-viewing Tropospheric Emission Spectrometer, *J. Geophys. Res. Atmos.*, *119*, 6971–6990, doi:10.1002/2013JD020822.
Ploeger, F., P. Konopka, R. Müller, S. Fueglistaler, T. Schmidt, J. C. Manners, J.-U. Grooß, G. Günther, P. M. Forster, and M. Riese (2012), Horizontal transport affecting trace gas seasonality in the Tropical Tropopause Layer (TTL), *J. Geophys. Res.*, *117*, D09303, doi:10.1029/2011JD017267.
Plumb, R. A. (1996), A "tropical pipe" model of stratospheric transport, *J. Geophys. Res.*, *101*, 3957–3972, doi:10.1029/95JD03002.
Randel, W. J., J. C. Gille, A. E. Roche, J. B. Kumer, J. L. Mergenthaler, J. W. Waters, E. F. Fishbein, and W. A. Lahoz (1993), Stratospheric transport from the tropics to middle latitudes by planetary-wave mixing, *Nature*, *365*, 533–535.
Remsberg, E. E., K. V. Haggard, and J. M. Russell (1990), Estimation of synoptic fields of middle atmosphere parameters from nimbus-7 LIMS profile data, *J. Atmos. Oceanic Technol.*, *7*, 689–705, doi:10.1175/1520-0426(1990)007<0689:EOSFOM>2.0.CO;2.
Rienecker, M. M., et al. (2011), MERRA: NASA's Modern-Era retrospective analysis for research and applications, *J. Clim.*, *24*(14), 3624–3648, doi:10.1175/JCLI-D-11-00015.1.
Rodgers, C. D. (1977), Statistical principles of inversion theory, in *Inversion Methods in Atmospheric Remote Sounding*, edited by A. Deepak, pp. 117–138, Academic Press, New York.
Rodgers, C. D. (2000), *Inverse Methods for Atmospheric Sounding; Theory and Practice*, World Scientific, London, isbn:981-02-2740-X.
Schoeberl, M. R., L. R. Lait, P. A. Newman, and J. E. Rosenfield (1992), The structure of the polar vortex, *J. Geophys. Res.*, *97*, 7859–7882, doi:10.1029/91JD02168.
Shepherd, T. G. (2007), Transport in the middle atmosphere, *J. Meteorol. Soc. Jpn.*, *85B*, 165–191.
Shuckburgh, E., W. Norton, A. Iwi, and P. Haynes (2001), Influence of the quasi-biennial oscillation on isentropic transport and mixing in the tropics and subtropics, *J. Geophys. Res.*, *106*(D13), 14,327–14,337, doi:10.1029/2000JD900664.
Strahan, S. E., and J. D. Mahlman (1994), Evaluation of the SKYHI general circulation model using aircraft measurements 1. Polar winter stratospheric meteorology and tracer morphology, *J. Geophys. Res.*, *99*, 10,305–10,318, doi:10.1029/93JD02332.
Tegtmeier, S., et al. (2013), SPARC data initiative: A comparison of ozone climatologies from international satellite limb sounders, *J. Geophys. Res. Atmos.*, *118*, 12,229–12,247, doi:10.1002/2013JD019877.
Volk, C. M., et al. (1996), Quantifying transport between the tropical and mid-latitude lower stratosphere, *Science*, *272*, 1763–1768.
Waters, J. W., et al. (2006), The earth observing system Microwave Limb Sounder (MLS) on the aura satellite, *IEEE Trans. Geosci. Remote Sens.*, *44*(5), 1075–1092.
WMO (1990), Report of the international ozone trends panel: 1988, *Rep*. 18, World Meteorol. Organ., Geneva.
Wright, C. J., M. B. Rivas, and J. C. Gille (2011), Intercomparisons of HIRDLS, COSMIC and SABER for the detection of stratospheric gravity waves, *Atmos. Meas. Tech.*, *4*, 1581–1591, doi:10.5194/amt-4-1581-2011.